

AUTOMOTIVE EXPERIENCES

Vol. 8 No. 2 (2025) pp. 353-368

p-ISSN: 2615-6202 e-ISSN: 2615-6636

# Research Paper

# Multi-Objective Optimization of Structural Design for Lightweight Vehicle Chassis

Dharma Maheswara¹, Poppy Puspitasari¹,² ☐, Diki Dwi Pramono¹, Avita Ayu Permanasari¹, Sukarni Sukarni¹

<sup>1</sup>Department of Mechanical and Industrial Engineering, Universitas Negeri Malang, Malang 65145, Indonesia <sup>2</sup>Centre of Advanced Material and Renewable Energy, Universitas Negeri Malang, Malang 65145, Indonesia

- poppy@um.ac.id
- https://doi.org/10.31603/ae.13567

Published by Automotive Laboratory of Universitas Muhammadiyah Magelang

#### **Abstract**

Article Info Submitted: 13/05/2025 Revised: 02/09/2025 Accepted: 02/09/2025 Online first: 25/09/2025 This study presents a systematic optimization of a lightweight vehicle chassis design using Design of Experiments (DoE), Finite Element Analysis (FEA), and Analysis of Variance (ANOVA) to enhance structural performance while balancing mass efficiency and safety factor. Material selection and wall thickness variations were considered to achieve a compromise between minimal mass and a safety factor of at least 1.5. Pareto front analysis, combined with the Taguchi method, identified the optimal solution, Cycle Design 11, which achieved a safety factor of 1.9489, representing an increase of 0.7681 compared to the baseline design. The total mass of 3.5742 kg reflects a 32.13% increase from the baseline. ANOVA results confirmed that both material and wall thickness significantly influence safety factor and mass, providing critical guidance for design decisions. This multi-objective optimization approach demonstrates that integrating FEA with experimental design enables superior chassis designs compared to traditional single-objective methods, offering a practical strategy for developing lightweight, safe, and energy-efficient vehicles.

**Keywords:** Design optimization; Lightweight chassis; Design of Experiments (DoE); Finite Element Analysis (FEA); Pareto optimal front

# 1. Introduction

Improving vehicle efficiency has become imperative to reducing energy consumption and the intensity of carbon emissions in the transportation industry [1], [2]. This is because global demand for passenger and freight transportation is expected to increase significantly by 196% and 200% between 2020 and 2050 [3]. The energy demand in the global transportation sector is expected to increase by nearly 4%, and total final energy consumption in the transportation sector is projected to be approximately 120 EJ in 2023 [4]. As much as 90% of this energy is provided by fossil oil-based fuels, 4% by biofuels, 5% by natural gas, and 1% by electricity. Since 1990, greenhouse gas emissions from the global

transportation sector have increased steadily at a rate of approximately 2% per year [5]. The increase in greenhouse gas emissions due to fossil energy is the primary trigger of global warming, pollution, and public health problems [6], [7]. Increasing fossil fuel consumption in the transportation sector is not in line with the principles of Sustainable Development Goals (SDGs) Goal 7 (Clean and Affordable Energy) [8].

Intensive study efforts aimed at improving vehicle energy efficiency in the world for students, one of which is the Shell Eco-marathon program [9]. The goal of the Shell Eco-marathon is the mileage challenge, which involves completing the race within the allotted time with the least energy consumption. Design and technology aspects, utilizing Science, Technology, Engineering, and



This work is licensed under a Creative Commons Attribution-NonCommercial 4.0 International License.

Maths (STEM) skills, are emphasized in this competition [10]. A common strategy to improve energy efficiency is to lighten the weight of the vehicle [11], [12]. Therefore, this study focuses on developing an optimal chassis design for prototype vehicles in the Shell Eco-marathon competition. The chassis is one of the most important parts of a vehicle, functioning like a human skeleton, where various components, such as the engine, drive system, brakes, body, and steering system, are mounted [13]. Designing the chassis is crucial to ensure the safety, performance, and durability of the vehicle, as well as to enhance vehicle handling and efficiency [14].

The study developed an optimization framework utilizing finite element analysis (FEA) for hybrid truck chassis, successfully reducing chassis mass by 13.25% while maintaining the allowable von Mises thereby stress, demonstrating the effectiveness of computational optimization in designing lightweight vehicle [15], [16], [17]. The study Nandhakumar et al. [18] is particulary interesting in this field, as they performed structural optimization (Topology, Size, and Shape) by modifying the existing material to achieve weight reduction of the chassis frame, thereby improving the overall performance of the bus. By replacing the steel in the chassis frame with aluminum 6061-T6 and aluminum 7075-T6, a weight reduction of 65.61% and 64.33% was achieved. FEA was performed on the chassis frame to ensure that safe stress limits were not exceeded. The study topic of Kengkongan et al. [19] is the effect of chassis thickness variation, the effect of different materials, and the impact of applied force values. The study aimed to evaluate the behavioral tendency of the vehicle chassis with the primary consideration of complying with standard energy-efficient regulations vehicle in competitions such as Shell Eco-marathon Asia or Kontes Mobil Hemat Energi (KMHE). The thickness of the chassis plays an important role in its performance. Moayyedian et al. [20] applied an optimization process to determine the optimal design for hubs and spindles in solar-powered vehicles using design of experiments (DoE) and FEA. Experiments were designed to achieve maximum safety and minimum weight. The spindle yielded a safety factor of 3.8 and a mass of 0.826 kg while the hub yielded a safety factor of

5.2 and a mass of 0.294 kg, indicating a reliable safety factor and a lightweight design. The recent study examining the use of aluminum 7075-T6 in car frames successfully reduced frame mass by approximately 40% while maintaining high strength and effective energy absorption during frontal collision simulations. Analysis shows that passenger zone deformation remains well below critical limits, highlighting the importance of incorporating safety factors into lightweight frame design to ensure passenger protection without compromising structural efficiency [21].

Despite extensive study on vehicle chassis optimization, existing studies primarily focus on isolated factors such as material selection, wall thickness, or individual component performance, without providing a systematic multi-objective framework that simultaneously addresses mass reduction and structural safety. To fill this gap, the present study develops an integrated optimization methodology combining DoE, FEA, and analysis of variance (ANOVA) to quantify the influence of material and geometric parameters on chassis performance. The proposed framework enables multi-objective optimization, identifying configurations that achieve significant chassis weight reduction while maintaining reliable safety factors, thereby improving both structural efficiency and occupant protection. This study contributes to the field by offering a validated, practical approach for lightweight chassis design in energy-efficient vehicle competitions and advancing the broader understanding computational optimization structural in automotive engineering.

### 2. Methods

#### 2.1. Material Selection

The selection of a suitable material for chassis design is based on factors such as strength, lightweight, ease of manufacturing, availability. Aluminum alloy is a widely selected material for lightweight structures in the automotive industry [18], [22]. As part of this study, two potential aluminum alloys were 6061-T6 selected, namely aluminum aluminum 7075-T6. Aluminum alloys established materials automotive for lightweighting due to their high specific strength or stiffness and corrosion resistance. Within this family, aluminum 6061-T6 is widely used for thinwalled structural members and energy absorbers, appears frequently in crash/impact investigations on tubes/extrusions-reflecting its weldability and suitability for spaceframe/chassis members [23], [24]. Aluminum 7075-T6 provides a substantially higher strength level and is often used as a high-strength benchmark in weight-critical members, including studies thin-walled tubes under dynamic/crash-type loading. These attributes align with our study's aims of minimizing mass while maintaining safety margins [25], [26]. Brief information about the composition of aluminum alloys is shown in Table 1. The mechanical properties of the materials used in the chassis design, aluminum 6061-T6 and aluminum 7075-T6, are shown in Table 2.

### 2.2. Physical Model

The ladder frame is one of the oldest chassis forms still used in many SUV vehicles. The ladder frame chassis design offers ease of production, cost efficiency, and high structural strength through the triangulated truss principle [13]. Therefore, the chassis design in this study adopts the ladder frame chassis design. The chassis geometry design utilizes Computer-Aided Design (CAD) software. The design of the chassis geometry is based on the regulations of the energy-efficient vehicle competition, considering design size limitations and load distribution. The chassis geometry design in this study comprises several supporting parts, and a hollow profile structure is selected for the geometry design. The chassis geometry design 3D model and technical drawing are shown in Figure 1.

# 2.3. Design of Experiment (DoE)

The DoE defines the factors, levels, and orthogonal array arrangement, specifying the combinations to be analyzed in the optimization process. The DoE matrix and subsequent ANOVA were generated and analyzed using Minitab 22.2 software, which allowed for the systematic identification of the dominant factors influencing chassis mass and safety factor. Optimization is

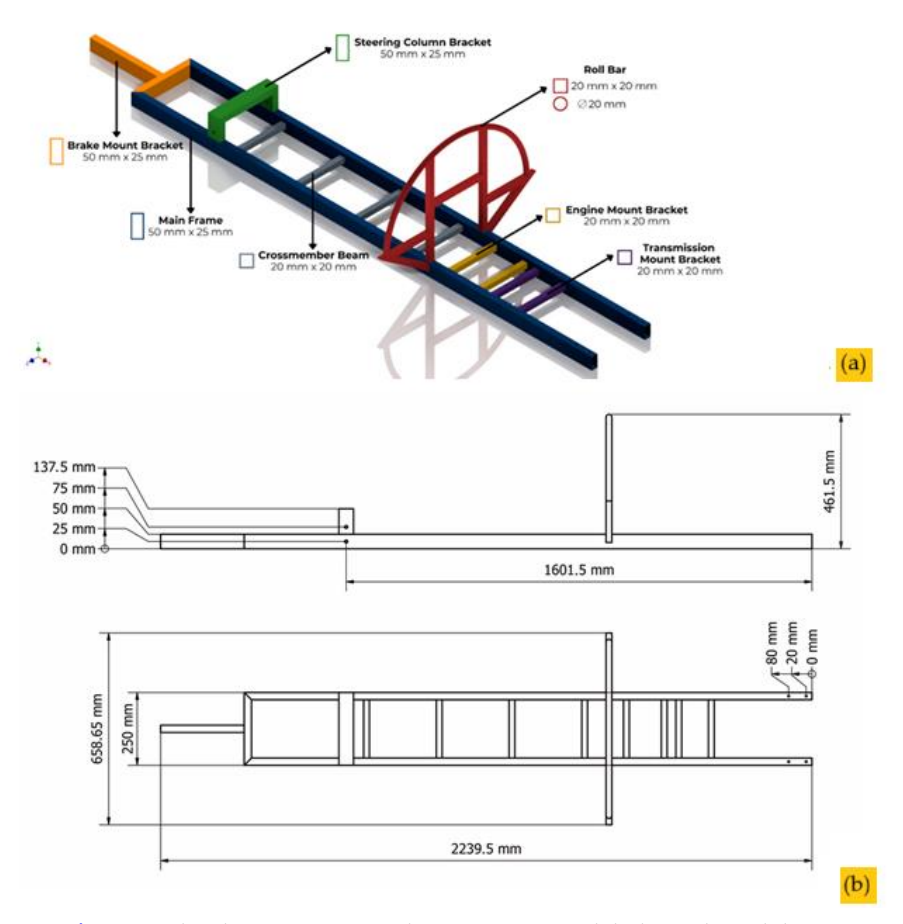


Figure 1. The chassis geometry design: (a) 3D model; (b) Technical drawing

Table 1. Composition of selected aluminum alloys [27]

| Allows -         | Composition (wt%) |           |      |         |         |      |           |     |     |
|------------------|-------------------|-----------|------|---------|---------|------|-----------|-----|-----|
| Alloys -         | Al                | Cu        | Mn   | Mg      | Zn      | Ti   | Cr        | Si  | Fe  |
| Aluminum 6061-T6 | 95.8-98.6         | 0.15 -0.4 | 0.15 | 0.8-1.2 | 0.25    | 0.15 | 0.04-0.35 | 0.4 | 0.7 |
| Aluminum 7075-T6 | 87.1-91.4         | 1.2 - 2   | 0.3  | 2.1-2.9 | 5.1-6.1 | 0.2  | 0.18-0.28 | 0.4 | 0.5 |

**Table 2**. Mechanical properties of selected aluminum alloys [27]

| Property                         | Aluminum 6061-T6 | Aluminum 7075-T6 | Unit  |
|----------------------------------|------------------|------------------|-------|
| Density                          | 2700             | 2810             | kg/m³ |
| Modulus of Elasticity            | 68900            | 71700            | MPa   |
| Poisson's Ratio                  | 0.33             | 0.33             | -     |
| Yield Tensile Strength           | 276              | 503              | MPa   |
| Ultimate Tensile Streght         | 310              | 572              | MPa   |
| Fatigue Strength (@ Cycles 5e+8) | 96.5             | 159              | MPa   |

carried out by applying variations in the wall thickness of the hollow profile, namely 1 mm, 2 mm, and 3 mm, to each constituent part of the chassis. The 1-3 mm range corresponds to the canonical thin-walled regime crashworthiness/energy-absorption studies, where progressive folding/buckling yields high specific energy absorption with manufacturable sections. Representative peer-reviewed examples include ~1.2 mm-wall aluminum tubes in impact/crashbox tests and ~3.15 mm-wall AA6061-T6 square tubes in crush experiments bracketing the design space explored in our [28], [29]. In addition to the optimization thickness factor, material variation is also considered as one of the optimization parameters. For the materials factor, aluminum 6061-T6 was designated as level 1, while aluminum 7075-T6 was designated as level 2 in the Taguchi-DoE matrix. The factors and levels used in the optimization scheme in this study are shown in Table 3. The experimental design in this study employs an orthogonal array L18 ( $2^1 \times 3^7$ ), which enables the control of one factor at two levels and seven other factors at three levels, resulting in a total of 18 test combinations. The L18 orthogonal

array design for the chassis optimization scheme is shown in

. In this study, the DoE is implemented prior to FEA to establish a structured optimization framework.

#### 2.4. Finite Element Analysis (FEA)

FEA is used to evaluate the structural response of chassis configurations determined by DoE. Each factor level combination is analyzed to obtain mass and safety factor values, which serve as quantitative inputs for Taguchi analysis. FEA divides the workpiece into small elements to analyze the response to applied forces under certain boundary conditions and produce a comprehensive output [30]. Structural analysis of components is a crucial step in the design phase, ensuring feasibility and reliability before the production stage [31], [32]. The design structure of the chassis is analyzed using a static approach, considering the main load of the vehicle at rest, where the load magnitude and direction are assumed to be fixed, enabling more stable and design predictions. This condition ensures that the chassis can maintain its structural

Table 3. Factors and levels of Taguchi-DoE

| Parameter | Unit | Process Parameter          | Level 1 | Level 2 | Level 3 |
|-----------|------|----------------------------|---------|---------|---------|
| A         | -    | Materials                  | 1       | 2       | -       |
| В         | mm   | Main Frame                 | 1       | 2       | 3       |
| С         | mm   | Crossmember Beam           | 1       | 2       | 3       |
| D         | mm   | Roll Bar                   | 1       | 2       | 3       |
| E         | mm   | Steering Column Bracket    | 1       | 2       | 3       |
| F         | mm   | Brake Mount Bracket        | 1       | 2       | 3       |
| G         | mm   | Engine Mount Bracket       | 1       | 2       | 3       |
| Н         | mm   | Transmission Mount Bracket | 1       | 2       | 3       |

|              | 0 | , . | , | 0 |   |   |   |   |
|--------------|---|-----|---|---|---|---|---|---|
| Cycle Design | A | В   | С | D | E | F | G | Н |
| 1            | 1 | 1   | 1 | 1 | 1 | 1 | 1 | 1 |
| 2            | 1 | 1   | 2 | 2 | 2 | 2 | 2 | 2 |
| 3            | 1 | 1   | 3 | 3 | 3 | 3 | 3 | 3 |
| 4            | 1 | 2   | 1 | 1 | 2 | 2 | 3 | 3 |
| 5            | 1 | 2   | 2 | 2 | 3 | 3 | 1 | 1 |
| 6            | 1 | 2   | 3 | 3 | 1 | 1 | 2 | 2 |
| 7            | 1 | 3   | 1 | 2 | 1 | 3 | 2 | 3 |
| 8            | 1 | 3   | 2 | 3 | 2 | 1 | 3 | 1 |
| 9            | 1 | 3   | 3 | 1 | 3 | 2 | 1 | 2 |
| 10           | 2 | 1   | 1 | 3 | 3 | 2 | 2 | 1 |
| 11           | 2 | 1   | 2 | 1 | 1 | 3 | 3 | 2 |
| 12           | 2 | 1   | 3 | 2 | 2 | 1 | 1 | 3 |
| 13           | 2 | 2   | 1 | 2 | 3 | 1 | 3 | 2 |
| 14           | 2 | 2   | 2 | 3 | 1 | 2 | 1 | 3 |
| 15           | 2 | 2   | 3 | 1 | 2 | 3 | 2 | 1 |
| 16           | 2 | 3   | 1 | 3 | 2 | 3 | 1 | 2 |
| 17           | 2 | 3   | 2 | 1 | 3 | 1 | 2 | 3 |
|              | _ | _   |   |   |   | _ | _ | _ |

Table 4. Orthogonal array design of Taguchi-DoE

integrity and support the load without experiencing significant deformation or failure [14]. Therefore, the FEA process in this study utilizes Computer-Aided Engineering (CAE) software with a static structural simulation type.

The pre-processing stage of static structural simulation includes CAD modeling, meshing, applying loads, and boundary conditions to the model [33]. The meshing stage is a crucial step in FEA, where appropriate structural assumptions are made to reduce computation time while ensuring model accuracy [31]. All chassis designs of the 18 test combinations were simulated using the same meshing parameters. The meshing parameters are set by default by the software, which adapts to the complexity of the chassis design and the computer's capabilities. Element

size was set to 15 mm. The meshing results show the dominance of the tetrahedral shape of 10. The tetrahedral meshing shape with 10 nodes exhibits reasonably high accuracy despite its smaller number of nodes, as well as simpler, lighter, and faster calculations [34]. Visualization of the meshing results on the chassis design is shown in Figure 2.

The application of boundary conditions in static structural simulations is crucial for accurately simulating the real physical conditions that influence the structural behavior of the chassis. All chassis designs from the 18 test combinations were simulated using the same boundary condition application to ensure objectivity and comparability. Table 5 presents details of the loads applied to the chassis used in

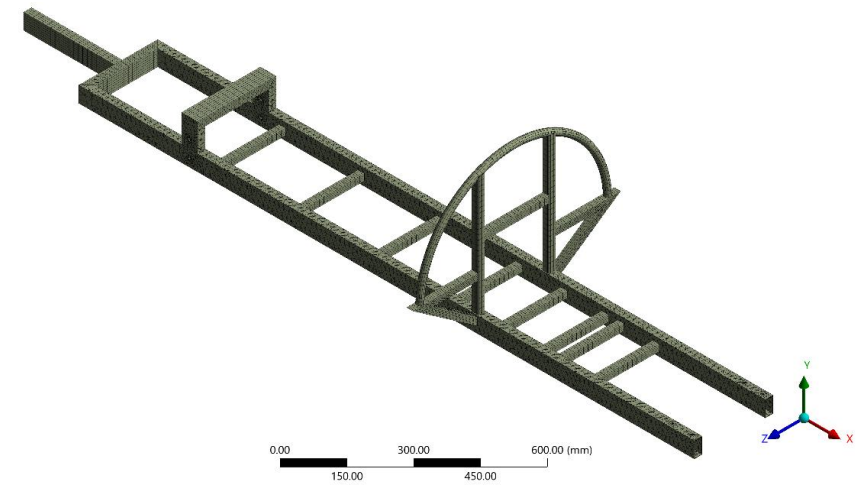


Figure 2. FEA meshing result

Table 5. Chassis loads in FEA

| No. | Components   | Load (kg) |
|-----|--------------|-----------|
| 1   | Driver       | 57        |
| 2   | Engine       | 20        |
| 3   | Transmission | 3         |
| 4   | Body         | 10        |
| 5   | Steering     | 2.5       |
| 6   | Brake        | 2         |
| 7   | Electrical   | 2         |
|     | Total        | 96.5      |

the simulation. Each mass value was subjected to gravitational acceleration ( $g = 9.8 \text{ m/s}^2$ ) in a downward direction in the negative direction of the Y-axis. The total applied load in **Table 5** corresponds to the prototype vehicle used in the Shell Eco-marathon competition, which is a lightweight vehicle with a total mass of approximately 96.5 kg, including the driver. This load was selected to represent the maximum expected static weight acting on the chassis during standard operation. Visualization of the boundary condition application is shown in **Figure 3**, which displays the position of the support and the direction of the force applied to the FEA model.

### 3. Results and Discussion

#### 3.1. Signal-to-Noise Ratio

All chassis design combinations in **Table 4** have undergone static structural simulation using FEA. The simulation results, including mass and safety factor, are shown in **Table 6**. The Taguchi method emphasizes the importance of analyzing response variation using the Signal-to-Noise (S/N) ratio

[35]. The mass value is transformed into an S/N ratio with "smaller the better" characteristics using Eq. (1). In comparison, the safety factor value is transformed into an S/N ratio with "larger the better" characteristics using Eq. (2). Eq. (1) and Eq. (2) for the S/N ratio were adopted from [36], [37].

$$SN_i = 10log\left(\sum_{u=1}^{N_i} \frac{y_u^2}{N_i}\right) \tag{1}$$

$$SN_i = 10log \left[ \frac{1}{N_i} \sum_{u=1}^{N_i} \frac{1}{y_u^2} \right]$$
 (2)

#### 3.2. Taguchi Analysis

To determine the critical factors that have a significant impact on the output parameters, the ANOVA technique was used [38]. The results of the ANOVA for mass are presented in Table 7. The main frame factor contributed the highest at 82.59%, followed by the roll bar at 9.05%, the brake mount bracket at 2.19%, the steering column bracket at 2.12%, and the crossmember beam at 1.68%. Other factors, such as the material, engine mount bracket, and transmission mount bracket, each contributed less than 1%, with a total contribution of 2.31%. Meanwhile, variables not examined in this study contributed 0.05% to the total variance.

The results of the level-to-mass response analysis are presented in **Table 8**. The highest level difference value indicates that the factor significantly influences the output parameters [20].

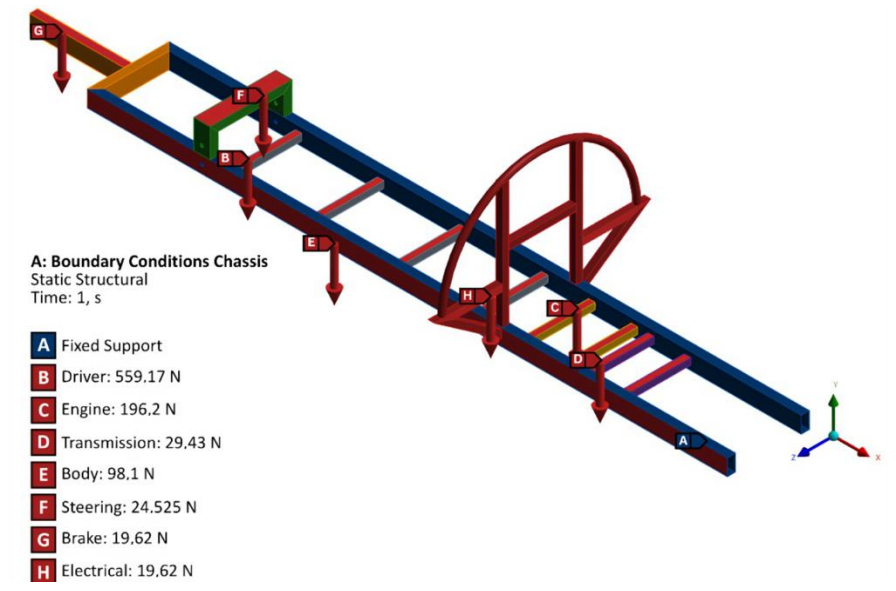


Figure 3. FEA boundary conditions

Table 6. Static structural simulation results with S/N ratio

| Cycle Design | Mass (kg) | Safety Factor | S/N Ratio Mass | S/N Ratio Safety Factor |
|--------------|-----------|---------------|----------------|-------------------------|
| 1            | 2.7049    | 1.1808        | -8.6430        | 1.4435                  |
| 2            | 3.7755    | 1.3509        | -11.5395       | 2.6125                  |
| 3            | 4.7398    | 1.3568        | -13.5152       | 2.6503                  |
| 4            | 4.7551    | 2.2992        | -13.5432       | 7.2315                  |
| 5            | 5.3831    | 2.4539        | -14.6206       | 7.7971                  |
| 6            | 5.4135    | 1.9386        | -14.6696       | 5.7498                  |
| 7            | 6.5384    | 2.4005        | -16.3094       | 7.6060                  |
| 8            | 6.7743    | 2.8738        | -16.6173       | 9.1691                  |
| 9            | 6.3243    | 3.3489        | -16.0202       | 10.4980                 |
| 10           | 4.2466    | 2.2353        | -12.5608       | 6.9867                  |
| 11           | 3.5742    | 1.9489        | -11.0636       | 5.7958                  |
| 12           | 3.8564    | 2.2269        | -11.7236       | 6.9540                  |
| 13           | 5.2839    | 4.0447        | -14.4591       | 12.1377                 |
| 14           | 5.689     | 3.196         | -15.1007       | 10.0921                 |
| 15           | 5.2125    | 3.7718        | -14.3409       | 11.5310                 |
| 16           | 7.2159    | 4.63          | -17.1658       | 13.3116                 |
| 17           | 6.3871    | 5.5685        | -16.1061       | 14.9148                 |
| 18           | 6.8288    | 4.0116        | -16.6869       | 12.0664                 |

Table 7. ANOVA results for the S/N ratio at mass

| Source                     | DF | Seq<br>SS | Adj<br>SS | Adj<br>MS | F-Value | P-Value | Contribution |
|----------------------------|----|-----------|-----------|-----------|---------|---------|--------------|
| Materials                  | 1  | 0.7727    | 0.7727    | 0.7727    | 37.06   | 0.026   | 0.85%        |
| Main Frame                 | 2  | 75.1469   | 75.1469   | 37.5735   | 1801.86 | 0.001   | 82.59%       |
| Crossmember Beam           | 2  | 1.5289    | 1.5289    | 0.7644    | 36.66   | 0.027   | 1.68%        |
| Roll Bar                   | 2  | 8.2372    | 8.2372    | 4.1186    | 197.51  | 0.005   | 9.05%        |
| Steering Column Bracket    | 2  | 1.9274    | 1.9274    | 0.9637    | 46.22   | 0.021   | 2.12%        |
| Brake Mount Bracket        | 2  | 1.9949    | 1.9949    | 0.9974    | 47.83   | 0.020   | 2.19%        |
| Engine Mount Bracket       | 2  | 0.6677    | 0.6677    | 0.3339    | 16.01   | 0.059   | 0.73%        |
| Transmission Mount Bracket | 2  | 0.6669    | 0.6669    | 0.3335    | 15.99   | 0.059   | 0.73%        |
| Residual Error             | 2  | 0.0417    | 0.0417    | 0.0209    |         |         | 0.05         |
| Total                      | 17 | 90.9843   |           |           |         |         | 100%         |

Table 8. Level response to mass

| Level | Materials       | Main Frame                 | Crossmember Beam    | Roll Bar                  |
|-------|-----------------|----------------------------|---------------------|---------------------------|
| 1     | -13.94          | -11.51                     | -13.78              | -13.29                    |
| 2     | -14.36          | -14.46                     | -14.17              | -14.22                    |
| 3     |                 | -16.48                     | -14.49              | -14.94                    |
| Delta | 0.41            | 4.98                       | 0.71                | 1.65                      |
| Rank  | 8               | 1                          | 5                   | 2                         |
| Level | Steering Column | <b>Brake Mount Bracket</b> | <b>Engine Mount</b> | <b>Transmission Mount</b> |
|       | Bracket         |                            | Bracket             | Bracket                   |
| 1     | -13.75          | -13.70                     | -13.88              | -13.91                    |
| 2     | -14.16          | -14.24                     | -14.25              | -14.15                    |
| 3     | -14.55          | -14.50                     | -14.31              | -14.38                    |
| Delta | 0.80            | 0.80                       | 0.44                | 0.47                      |
| Rank  | 3               | 4                          | 7                   | 6                         |

Based on the delta value of each factor, the main frame shows the highest value difference of 4.98, ranking first as the most influential factor on mass. The next factor is the roll bar with a delta value of 1.65, followed by the steering column bracket and

brake mount bracket, which have delta values of 0.80 and are ranked third and fourth, respectively. The crossmember beam factor ranked fifth with a delta of 0.71, while the transmission mount bracket and engine mount bracket had less

influence with deltas of 0.47 and 0.44, ranking sixth and seventh. The material factor has the smallest delta value of 0.41, so it is ranked eighth.

Based on the main effect graph shown in Figure 4, the combination of using aluminum 6061-T6 material on all parts of the chassis with a hollow profile wall thickness of 1 mm produces the highest Signal-to-Noise (S/N) ratio. This indicates the most optimal configuration for chassis design with the lowest mass. The ANOVA results in Table 7 indicate that the material factor accounts for 0.85% of the chassis design mass in this study. Although this value is relatively small, the material factor is still significant to consider in the context of chassis design optimization. Differences mainly influence this contribution in material density, where aluminum 7075-T6 has a density approximately 4% higher than aluminum 6061-T6 in identical geometries, resulting in a greater total mass [39]. In addition, the ANOVA results indicate that the thickness of the main frame is the most significant factor influencing the chassis mass in this study, accounting for 82.59% of the total variation. This finding is consistent with the structural principle that increasing thickness directly increases material volume and mass, as emphasized in the ladder frame chassis design literature, which highlights thickness optimization as a key factor in achieving weight reduction while maintaining rigidity for vehicle stability [40]. The next factor is the roll bar, which contributes 9.05%, reflecting the mass penalty due to the addition of rollover protection elements, in line with commercial vehicle chassis optimization studies [41]. Meanwhile, other components such as the brake mount bracket, steering column bracket, and crossmember beam have a more minor but still significant effect on mass accumulation.

The results of the ANOVA for safety factors are presented in **Table 9**. Based on the contribution analysis, the main frame factor contributed the most, 59.74%. The materials factor contributed 34.34%, while the steering column bracket contributed 5.23%. The other factors, including the crossmember beam, roll bar, brake mount bracket, engine mount bracket, and transmission mount bracket, each contributed less than 0.50%.

The results of the level-to-safety factor response analysis are presented in Table 10. Based on the delta value of each factor, the main frame shows the highest value difference of 6.854, ranking first as the most influential factor on the safety factor. The next factor is materials with a delta value of 4.337, followed by the steering column bracket and roll bar, which have values of 2.039 and 0.576, ranking third and fourth, respectively. The brake mount bracket factor ranked fifth with a delta of 0.280, while the crossmember beam (delta 0.277) and transmission mount bracket (delta 0.185) ranked sixth and seventh. The engine mount bracket factor has the least influence, with a delta of 0.174, ranking eighth.

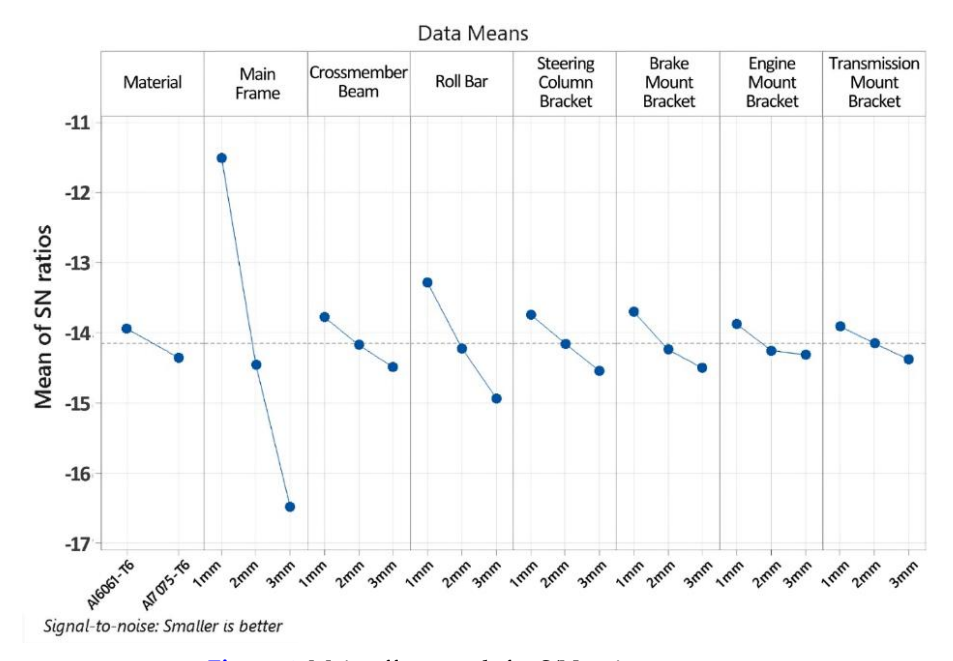


Figure 4. Main effect graph for S/N ratio at mass

Table 9. ANOVA results for the S/N ratio at safety factor

| Source                     | DF | Seq<br>SS | Adj<br>SS | Adj<br>MS | F-<br>Value | P-Value | Contribution |
|----------------------------|----|-----------|-----------|-----------|-------------|---------|--------------|
| Materials                  | 1  | 84.639    | 84.639    | 84.6393   | 806270.43   | 0.000   | 34.34%       |
| Main Frame                 | 2  | 147.234   | 147.234   | 73.6171   | 701272.96   | 0.000   | 59.74%       |
| Crossmember Beam           | 2  | 0.232     | 0.232     | 0.1160    | 1104.64     | 0.001   | 0.09%        |
| Roll Bar                   | 2  | 1.024     | 1.024     | 0.5120    | 4877.35     | 0.000   | 0.42%        |
| Steering Column Bracket    | 2  | 12.885    | 12.885    | 6.4425    | 61371.34    | 0.000   | 5.23%        |
| Brake Mount Bracket        | 2  | 0.235     | 0.235     | 0.1173    | 1117.31     | 0.001   | 0.10%        |
| Engine Mount Bracket       | 2  | 0.094     | 0.094     | 0.0472    | 449.79      | 0.002   | 0.04%        |
| Transmission Mount Bracket | 2  | 0.104     | 0.104     | 0.0520    | 495.80      | 0.002   | 0.04%        |
| Residual Error             | 2  | 0.000     | 0.000     | 0.0001    |             |         |              |
| Total                      | 17 | 246.448   |           |           |             |         | 100%         |

Table 10. Level response to safety factor

|       |                 | Tuble 10. Level resp | onse to safety factor |                           |
|-------|-----------------|----------------------|-----------------------|---------------------------|
| Level | Materials       | Main Frame           | Crossmember Beam      | Roll Bar                  |
| 1     | 6.084           | 4.407                | 8.120                 | 8.569                     |
| 2     | 10.421          | 9.090                | 8.397                 | 8.196                     |
| 3     |                 | 11.261               | 8.242                 | 7.993                     |
| Delta | 4.337           | 6.854                | 0.277                 | 0.576                     |
| Rank  | 2               | 1                    | 6                     | 4                         |
| Level | Steering Column | <b>Brake Mount</b>   | <b>Engine Mount</b>   | <b>Transmission Mount</b> |
|       | Bracket         | Bracket              | Bracket               | Bracket                   |
| 1     | 7.126           | 8.395                | 8.349                 | 8.166                     |
| 2     | 8.468           | 8.248                | 8.233                 | 8.351                     |
| 3     | 9.164           | 8.115                | 8.175                 | 8.241                     |
| Delta | 2.039           | 0.280                | 0.174                 | 0.185                     |
| Rank  | 3               | 5                    | 8                     | 7                         |

Meanwhile, the main effect graph shown in Figure 5 indicates the highest S/N ratio for the safety factor obtained by combining the use of aluminum 7075-T6 material on all chassis parts, including a hollow profile with a 3 mm wall thickness on the main frame and steering column bracket. And with a hollow profile wall thickness of 2 mm in the crossmember beam and transmission mount bracket. For the roll bar, brake mount bracket, and engine mount bracket, a 1 mm hollow profile wall thickness is sufficient. The combination of chassis design is the optimum condition to achieve the highest safety factor. The ANOVA results in Table 9 indicate that main frame thickness is the dominant parameter influencing the chassis safety factor, contributing 59.74% of the variance, followed by material selection at 34.34%. Collectively, these two factors account for over 94% of the response variation, underscoring their critical role in structural integrity. Thickening the main frame enhances stiffness and load-bearing capacity, thereby preventing stress concentrations, while selecting aluminum 7075-T6, which has a superior yield strength compared to aluminum 6061-T6, safety margins are inherently increased. The steering column bracket contributes 5.23% to the variance, as in the chassis design of this study, it functions as a fixed support for the knuckle arm mounting, making it susceptible to local stress peaks during dynamic loading. Optimizing this area is very crucial to prevent local failures. These results align with literature emphasizing the combined importance of material strength and frame geometry in enhancing chassis rigidity and safety, and the critical role of load transfer interfaces in preventing localized failure [39], [42].

### 3.3. Multi-Objective Optimization

The selection of the Pareto Optimal front method in this study is based on the complexity of the chassis design which involves two conflicting objectives, minimizing mass and maximizing the safety factor. Unlike single-objective optimization, which yields only a single solution, multiobjective design optimization approaches enable

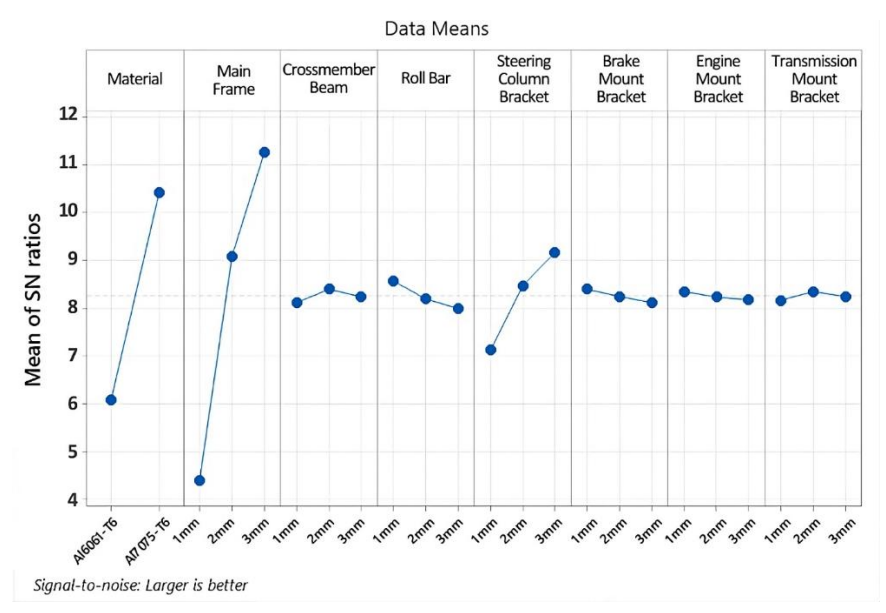


Figure 5. Main effect graph for S/N ratio at safety factor

the exploration of non-dominated solutions that are more representative of design compromises [43]. All these multi-objective design optimization solutions are collectively known as Pareto Optimal, and the path connecting these solutions in the search space is called the Pareto front [44], [45]. The selection of the optimal result of chassis design by this Pareto Optimal front method ensures the design decision is more holistic, data-driven, and follows modern structural optimization principles.

Figure 6 shows the Pareto front plot of the relationship between mass parameters and safety factor for each combination of chassis designs in this study. The red data points represent the optimal solution set for the chassis design in this study. This set of solutions represents the best compromise without sacrificing any of the parameters to the extreme. Mass minimization is a crucial aspect in high-efficiency or energyefficient vehicles as it directly reduces energy consumption and improves the acceleration performance and dynamic efficiency [46], [47]. Decreased energy consumption also contributes to reducing carbon emissions [48]. On the other hand, a minimum safety factor of 1.5 is used as a safe threshold to ensure tolerance to load variations, material uncertainties, and unexpected operational conditions that are common in dynamic environments [49], [50], [51].

Therefore, the optimal design selection in this study is based on a compromise point that minimizes mass while still meeting the minimum safety factor requirement of 1.5 or greater. Cycle Design 11 was selected as the optimal result in this study, and this chassis design combination has a mass of 3.5742 kg with a safety factor of 1.9489. The selected chassis design exhibits an increase in safety factor of up to 0.7681 compared to the baseline (Cycle Design 1), resulting in a corresponding increase in mass of 32.13%. In vehicle design, structural safety priorities often favor increased strength even at the expense of some weight efficiency, especially for applications that require higher resistance to dynamic or shock loads [52], [53], [54].

# 3.4. FEA Analysis Cycle Design 11

FEA results in Cycle Design 11 aim to evaluate significant structural performance based on safety factor, equivalent stress, and total deformation parameters to ensure the design meets technical

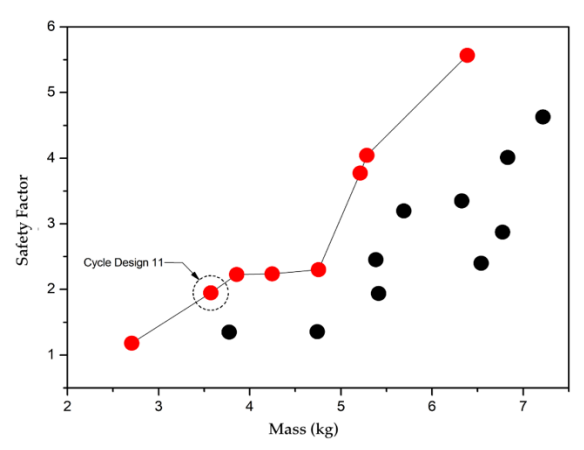


Figure 6. Plot pareto front

and functional criteria [55], [56]. Based on Figure 7, the chassis design yields a minimum safety factor of 1.9489, indicating that the chassis structure can withstand loads without failure, in with design accordance principles prioritizestructural integrity and safety [13]. The use of Equivalent (von Mises) Stress analysis in FEA to evaluate structural performance is based on Distortion Energy Theory, which states that failure of ductile materials occurs when the distortion energy reaches a critical value, as in the one-way tensile test. Equivalent (von Mises) Stress is a failure criterion that considers the combined effect of principal stresses in three directions under various complex loading conditions in numerical simulations [57], [58]. Based on Figure 8, the analysis results show a maximum stress of 81.586 MPa, well below the yield strength (503 MPa) and ultimate tensile strength (572 MPa) of the aluminum 7075-T6 material. These results indicate that the chassis structure is operating within elastic limits and is safe against the risk of permanent deformation or material failure [59]. Figure 9 shows the maximum deformation value of 1.5141 mm, which occurs in the negative direction of the Y axis of the chassis design. This indicates the degree of flexure or deflection of the chassis structure against vertical loads such as the mass of the driver and vehicle components. Significant structural deflection can lower the natural frequency of the chassis and trigger resonance due to excitation from the road surface, negatively affecting vehicle comfort, stability, and efficiency [60]. In contrast, low vertical deformations, as in these results, reflect good structural performance and support the vehicle's dynamic stability.

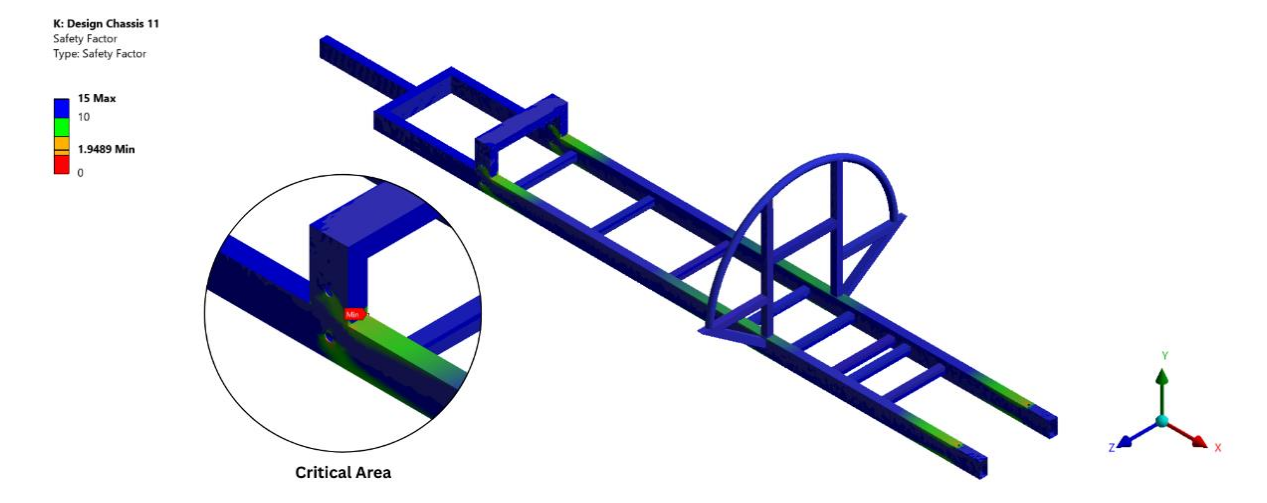


Figure 7. Safety factor cycle design 11

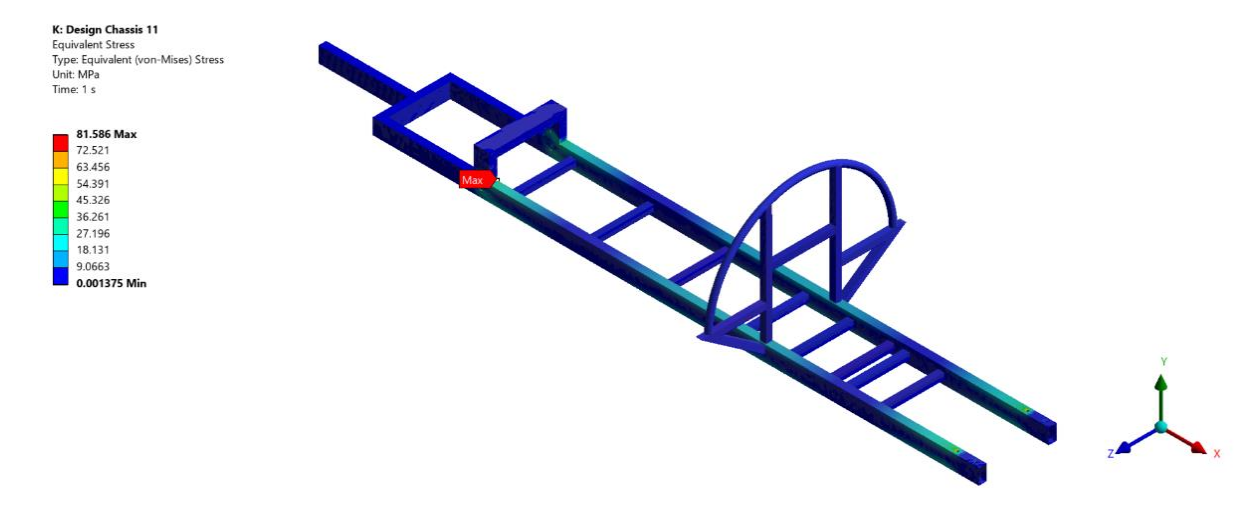


Figure 8. Equivalent stress cycle design 11

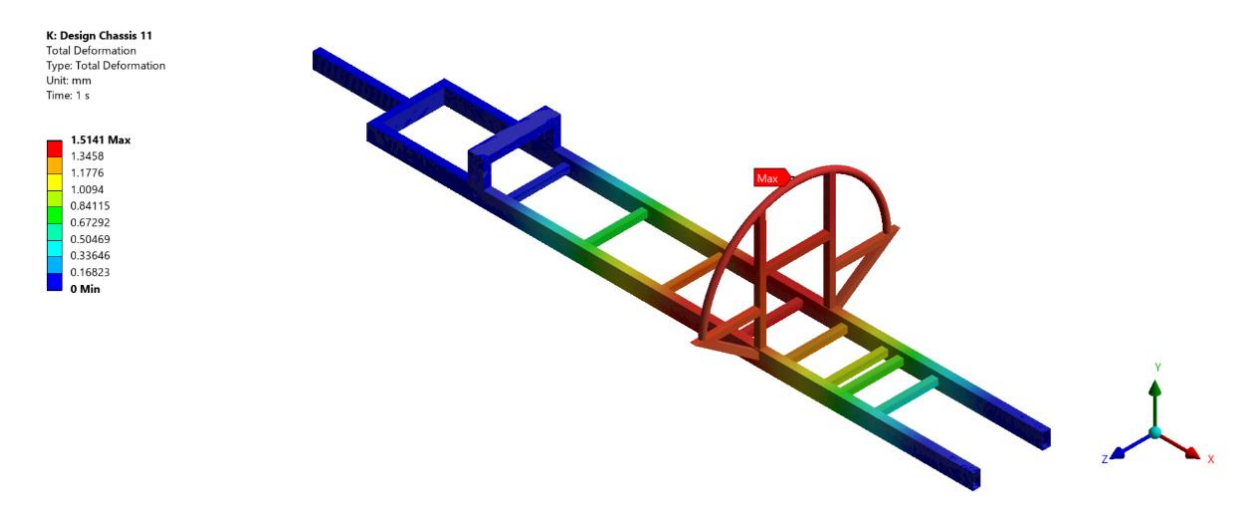


Figure 9. Total deformation cycle design 11

#### 4. Conclusion

This study successfully integrated DoE, FEA, and ANOVA to optimize the design of a light vehicle chassis. The primary objective was to achieve an optimal balance between mass efficiency and structural safety while ensuring overall chassis integrity under operational loads. FEA simulations demonstrated that the selected optimal chassis configuration, Cycle Design 11, achieved a minimum safety factor of 1.9489, representing an increase of 0.7681 compared to the baseline design (Cycle Design 1). corresponding chassis mass is 3.5742 kg, reflecting a 32.13% increase from the baseline, which is considered acceptable given the improved structural robustness. The maximum stress was 81.586 MPa, well below the yield and ultimate strengths of aluminum 7075-T6. tensile behavior confirming elastic under load. Meanwhile, the maximum deformation reached 1.5141 mm along the negative Y-axis, indicating that the chassis can sustain vertical loads without significantly impacting stability or dynamic performance. Using multi-objective a optimization approach and Pareto front analysis, the study identified a set of compromise solutions that balance mass minimization with a safety factor above the recommended threshold of 1.5. Cycle Design 11 represents the most favorable compromise, ensuring adequate structural safety without excessive mass penalty. This optimization highlights the importance of material selection and thickness variation, as demonstrated by Taguchi methods and ANOVA, in influencing chassis performance. Overall, this work provides a comprehensive approach to light vehicle chassis combining advanced design, simulation techniques with experimental design The findings offer valuable methodologies. insights for future energy-efficient vehicle development, demonstrating that chassis designs can be optimized to maintain safety and structural integrity while improving efficiency and reducing environmental impact.

# Acknowledgements

The authors would like to thank all those who have helped this research, especially the Energy Efficient Vehicle Team of Universitas Negeri Malang, Center of Advanced Materials and Renewable Energy.

#### **Author's Declaration**

# Authors' contributions and responsibilities

The authors made substantial contributions to the conception and design of the study. The authors took responsibility for data analysis, interpretation and discussion of results. The authors read and approved the final manuscript.

#### **Funding**

No funding information from the authors.

#### Availability of data and materials

All data are available from the authors.

#### **Competing interests**

The authors declare no competing interest.

#### Additional information

No additional information from the authors.

#### References

- [1] A. Cheng *et al.*, "Changes in low-carbon transportation efficiency of Chinese roads after considering the impact of new energy vehicles," *Transport Policy*, vol. 159, pp. 28–43, Dec. 2024, doi: 10.1016/j.tranpol.2024.09.020.
- [2] W. Achariyaviriya, W. Wongsapai, D. Rinchumphu, N. Tippayawong, K. Y. Tippayawong, and P. Suttakul, "A comparative study of vehicle powertrain efficiency: Data-driven analyzing energy consumption and environmental impact," *Transportation Engineering*, vol. 18, p. 100286, Dec. 2024, doi: 10.1016/j.treng.2024.100286.
- [3] S. Tjandra *et al.*, "Model-based analysis of future global transport demand," *Transportation Research Interdisciplinary Perspectives*, vol. 23, p. 101016, Jan. 2024, doi: 10.1016/j.trip.2024.101016.
- [4] International Energy Agency, "World Energy Outlook," 2024. [Online]. Available: https://www.iea.org/reports/world-energy-outlook-2024
- [5] W. F. Lamb *et al.*, "A review of trends and drivers of greenhouse gas emissions by sector from 1990 to 2018," *Environmental Research Letters*, vol. 16, no. 7, p. 073005, Jul. 2021, doi: 10.1088/1748-9326/abee4e.
- [6] Y. Lan, H. Gao, P. Zhou, H. Zhang, and H. Li, "The impact of climate risks on global energy production and consumption: New evidence from causality-in-quantile and wavelet analysis," *Energy*, vol. 319, p. 134850, Mar. 2025, doi: 10.1016/j.energy.2025.134850.
- [7] H. H. Abdulkadhim Altaee, F. Rahim, K. Dzhusupov, and K. Toguzbaeva, "Impact of CO2 emissions, income, and urbanization on health status in GCC countries: A moderating role of energy consumption," *Global Transitions*, vol. 7, pp. 211–222, 2025, doi: 10.1016/j.glt.2025.04.005.
- [8] R. Madurai Elavarasan *et al.*, "The untold subtlety of energy consumption and its influence on policy drive towards Sustainable Development Goal 7," *Applied Energy*, vol. 334, p. 120698, Mar. 2023, doi: 10.1016/j.apenergy.2023.120698.
- [9] Z. Pusztai, P. Kőrös, F. Szauter, and F.

- Friedler, "Vehicle Model-Based Driving Strategy Optimization for Lightweight Vehicle," *Energies*, vol. 15, no. 10, p. 3631, May 2022, doi: 10.3390/en15103631.
- [10] Shell, "Shell Eco-Marathon 2025 Official Rules, Chapter I," Shell. [Online]. Available: https://www.shellecomarathon.com/about/g lobal-rules.html
- [11] M. Choi, J. Cha, and J. Song, "Impact of lightweighting and driving conditions on electric vehicle energy consumption: Indepth analysis using real-world testing and simulation," *Energy*, vol. 323, p. 135746, May 2025, doi: 10.1016/j.energy.2025.135746.
- [12] G. Refiadi, I. S. Aisyah, and J. P. Siregar, "Trends in Lightweight Automotive Materials for Improving Fuel Efficiency and Reducing Carbon Emissions," *Automotive Experiences*, vol. 2, no. 3, pp. 78–90, Oct. 2019, doi: 10.31603/ae.v2i3.2984.
- [13] I. A. Majid, F. B. Laksono, H. Suryanto, and A. R. Prabowo, "Structural Assessment of Ladder Frame Chassis using FE Analysis: A Designed Construction referring to Ford AC Cobra," *Procedia Structural Integrity*, vol. 33, pp. 35–42, 2021, doi: https://doi.org/10.1016/j.prostr.2021.10.006.
- [14] N. N. Tien, H. N. Van, V. N. Duy, and H. P. Trinh, "Simulation-based comparative analysis of different chassis configurations of hybrid fuel cell vehicle," *International Journal of Thermofluids*, vol. 24, p. 100968, Nov. 2024, doi: 10.1016/j.ijft.2024.100968.
- [15] S. De *et al.*, "Lightweight Chassis Design of Hybrid Trucks Considering Multiple Road Conditions and Constraints," *World Electric Vehicle Journal*, vol. 12, no. 1, p. 3, Dec. 2020, doi: 10.3390/wevj12010003.
- [16] H. S. Hanandita, U. Ubaidillah, A. R. Prabowo, B. W. Lenggana, A. Turnip, and E. Joelianto, "Static Structural Analysis of Checking Fixture Frame of Car Interior Using Finite Element Method," *Automotive Experiences*, vol. 6, no. 3, pp. 652–668, Dec. 2023, doi: 10.31603/ae.9860.
- [17] R. P. Putra *et al.*, "Design and Crash Test on a Two-Passenger City Car Frame using Finite Element Method," *Automotive Experiences*, vol. 7, no. 2, pp. 270–283, Sep. 2024, doi: 10.31603/ae.11306.

- [18] S. Nandhakumar, S. Seenivasan, A. M. Saalih, and M. Saifudheen, "Materials Today: Proceedings Weight optimization and structural analysis of an electric bus chassis frame," *Materials Today: Proceedings*, no. x, 2020, doi: 10.1016/j.matpr.2020.07.404.
- [19] A. Kengkongan, A. Rio, and F. Imaduddin, "Structural assessment of an energy-efficient urban vehicle chassis using finite element analysis A case study," *Procedia Structural Integrity*, vol. 27, no. 2019, pp. 69–76, 2020, doi: 10.1016/j.prostr.2020.07.010.
- [20] M. Moayyedian *et al.*, "DoE-FEM Based Design Optimization of Hub and Spindle," *Procedia CIRP*, vol. 119, pp. 47–51, 2023, doi: 10.1016/j.procir.2023.01.001.
- [21] U. Idrees *et al.*, "Finite element analysis of car frame frontal crash using lightweight materials," *Journal of Engineering Research*, vol. 11, no. 1, p. 100007, Mar. 2023, doi: 10.1016/j.jer.2023.100007.
- [22] S. Saifudin, N. Muhayat, E. Surojo, Y. H. Manurung, and T. Triyono, "Mitigation of Porosity and Residual Stress on Carbody Aluminum Alloy Vibration Welding: A Systematic Literature Review," *Automotive Experiences*, vol. 5, no. 3, pp. 477–493, Nov. 2022, doi: 10.31603/ae.7965.
- [23] H. Ma, K. Lu, and X. Liu, "Experimental and numerical studies on lateral low-velocity impact behaviour and residual axial strength of circular aluminum alloy (6061-T6) tubes," *Structures*, vol. 47, pp. 1250–1264, Jan. 2023, doi: 10.1016/j.istruc.2022.11.017.
- [24] S. Bhutada and M. D. Goel, "Progressive axial crushing behaviour of Al6061-T6 alloy tubes with geometrical modifications under impact loading," *Thin-Walled Structures*, vol. 182, p. 110240, Jan. 2023, doi: 10.1016/j.tws.2022.110240.
- [25] P. Kaczyński, "Crashworthiness Characteristic of Dynamically Expanded Circular Tubes Made of Light Alloys: Experimental and Theoretical Investigation," *Materials*, vol. 13, no. 23, p. 5332, Nov. 2020, doi: 10.3390/ma13235332.
- [26] M. Tisza and I. Czinege, "Comparative study of the application of steels and aluminium in lightweight production of automotive parts," International Journal of Lightweight Materials

- *and Manufacture*, vol. 1, no. 4, pp. 229–238, Dec. 2018, doi: 10.1016/j.ijlmm.2018.09.001.
- [27] ASM Handbook Committee, *Properties and Selection: Nonferrous Alloys and Special-Purpose Materials*. ASM International, 1990. doi: 10.31399/asm.hb.v02.9781627081627.
- [28] M. Rogala, M. Ferdynus, K. Gawdzińska, and P. Kochmański, "The Influence of Different Length Aluminum Foam Filling on Mechanical Behavior of a Square Thin-Walled Column," *Materials*, vol. 14, no. 13, p. 3630, Jun. 2021, doi: 10.3390/ma14133630.
- [29] Q. Cheng, W. Altenhof, and L. Li, "Experimental investigations on the crush behaviour of AA6061-T6 aluminum square tubes with different types of through-hole discontinuities," *Thin-Walled Structures*, vol. 44, no. 4, pp. 441–454, Apr. 2006, doi: 10.1016/j.tws.2006.03.017.
- [30] Rohit Singh, D. S. Gupta, Beohar, and D. Gouraw, "Optimizing T4 Class Vehicle Chassis Designs: A Finite Element Method Analysis Using Solid Edge 2022 and ANSYS 24.0," International Research Journal of Modernization in Engineering Technology and Science, vol. 6, no. 6, Apr. 2024, doi: 10.56726/IRJMETS52217.
- [31] A. C. Ram Kumar, N. Mohammed Raffic, K. Ganesh Babu, and S. Selvakumar, "Static structural analysis of spur gear using ANSYS 15.0 and material selection by COPRAS, MOORA techniques," *Materials Today: Proceedings*, vol. 47, pp. 25–36, 2021, doi: 10.1016/j.matpr.2021.03.485.
- [32] K. A. Rezkita, A. Kurniawan, and S. D. Anastasia Filias Tanira, "Structural strength evaluation of a modular toddler bicycle: Frame design and material considerations for children's progressive development," *Mechanical Engineering for Society and Industry*, vol. 5, no. 1, 2025, doi: 10.31603/mesi.12961.
- [33] A. Agarwal and L. Mthembu, "Numerical Modelling and Multi Objective Optimization Analysis of Heavy Vehicle Chassis," *Processes*, vol. 9, no. 11, p. 2028, Nov. 2021, doi: 10.3390/pr9112028.
- [34] A. K. Ary *et al.*, "Numerical estimation of the torsional stiffness characteristics on urban Shell Eco-Marathon (SEM) vehicle design,"

- *Curved and Layered Structures*, vol. 8, no. 1, pp. 167–180, Jan. 2021, doi: 10.1515/cls-2021-0016.
- [35] P. Puspitasari, Suprayitno, R. Nurmalasari, D. D. Pramono, and A. K. Muhlasin, "Experimental and optimization of die casting parameters on Al-Si alloy with snail shell reinforcing agent," *Materials Research Express*, vol. 10, no. 12, p. 126517, Dec. 2023, doi: 10.1088/2053-1591/ad176f.
- [36] M. B. Silva, L. M. Carneiro, J. P. A. Silva, I. dos Santos Oliveira, H. J. I. Filho, and C. R. de Oliveira Almeida, "An Application of the Method (Robust Design) Taguchi Environmental Engineering: **Evaluating** Advanced Oxidative Processes in Polyester-Resin Wastewater Treatment," American Journal of Analytical Chemistry, vol. 05, no. 13, 828-837. 2014. pp. doi: 10.4236/ajac.2014.513092.
- [37] I. Ben Romdhane, A. Jemmali, S. Kaziz, F. Echouchene, T. Alshahrani, and H. Belmabrouk, "Taguchi method: artificial neural network approach for the optimization of high-efficiency microfluidic biosensor for COVID-19," *European Physical Journal Plus*, vol. 138, no. 4, 2023, doi: 10.1140/epip/s13360-023-03988-1.
- [38] R. Aslam, A. A. Khan, H. Akhtar, S. Saleem, and M. S. Ali, "Optimizing injection molding parameters to reduce weight and warpage in PET preforms using Taguchi method and Analysis of Variance (ANOVA)," *Next Materials*, vol. 8, no. November 2024, p. 100623, 2025, doi: 10.1016/j.nxmate.2025.100623.
- [39] M. Y. Khalid, R. Umer, and K. A. Khan, "Review of recent trends and developments in aluminium 7075 alloy and its metal matrix composites (MMCs) for aircraft applications," *Results in Engineering*, vol. 20, no. March, p. 101372, 2023, doi: 10.1016/j.rineng.2023.101372.
- [40] D. Shammy and R. V. Prakash, "Parametric Analysis of Factors Influencing Stiffness and Crashworthiness of a Ladder Frame," in *Volume 12: Transportation Systems*, American Society of Mechanical Engineers, Nov. 2016. doi: 10.1115/IMECE2016-65408.
- [41] P. Seyfried, E. J. M. Taiss, A. C. Calijorne, F. P. Li, and Q. F. Song, "Light weighting

- opportunities and material choice for commercial vehicle frame structures from a design point of view," *Advances in Manufacturing*, vol. 3, no. 1, pp. 19–26, 2015, doi: 10.1007/s40436-015-0103-8.
- [42] M. Hoffmann, S. Skibicki, P. Pankratow, A. Zieliński, M. Pajor, and M. Techman, "Automation in the Construction of a 3D-Printed Concrete Wall with the Use of a Lintel Gripper," *Materials*, vol. 13, no. 8, p. 1800, Apr. 2020, doi: 10.3390/ma13081800.
- [43] S. K. Sharma, B. K. Mishra, and I. V. Singh, "A multiobjective optimization framework based on FEA, ANN, and NSGA-II to optimize the process parameters of tube-to-tubesheet joint," *Finite Elements in Analysis and Design*, vol. 241, no. February, p. 104225, 2024, doi: 10.1016/j.finel.2024.104225.
- [44] J. Liu, J. Liu, X. Yan, and B. Peng, "A heuristic algorithm combining Pareto optimization and niche technology for multi-objective unequal area facility layout problem," *Engineering Applications of Artificial Intelligence*, vol. 89, no. November 2019, p. 103453, 2020, doi: 10.1016/j.engappai.2019.103453.
- [45] N. M. Okasha, A. K. Alzo'ubi, O. Mughieda, M. Kewalramani, and A. H. Almasri, "A near-optimum multi-objective optimization approach for structural design," *Ain Shams Engineering Journal*, vol. 15, no. 2, p. 102388, 2024, doi: 10.1016/j.asej.2023.102388.
- [46] M. S. Sarfraz, H. Hong, and S. S. Kim, "Recent developments in the manufacturing technologies of composite components and their cost-effectiveness in the automotive industry: A review study," *Composite Structures*, vol. 266, no. March, p. 113864, 2021, doi: 10.1016/j.compstruct.2021.113864.
- [47] W. Zhang and J. Xu, "Advanced lightweight materials for Automobiles: A review," *Materials & Design*, vol. 221, p. 110994, Sep. 2022, doi: 10.1016/j.matdes.2022.110994.
- [48] D. He, V. K. Soo, H. C. Kim, and M. Doolan, "Life Cycle Primary Energy Demand and Greenhouse Gas Emission benefits of vehicle lightweighting with recycled carbon fibre," *Procedia CIRP*, vol. 98, no. March, pp. 43–48, 2021, doi: 10.1016/j.procir.2021.01.003.
- [49] B. C. Rao, "Revisiting classical design in

- engineering from a perspective of frugality," *Heliyon*, vol. 3, no. 5, p. e00299, 2017, doi: 10.1016/j.heliyon.2017.e00299.
- [50] F. M. Burdekin, "General principles of the use of safety factors in design and assessment," *Engineering Failure Analysis*, vol. 14, no. 3, pp. 420–433, 2007, doi: 10.1016/j.engfailanal.2005.08.007.
- [51] X. Wang, Q. Shi, W. Fan, R. Wang, and L. Wang, "Comparison of the reliability-based and safety factor methods for structural design," *Applied Mathematical Modelling*, vol. 72, pp. 68–84, 2019, doi: 10.1016/j.apm.2019.03.018.
- [52] Y. Su, J. Zou, Z. Y. Li, and W. Lu, "Factors influencing the dynamic response of protective structures within heavy-duty vehicles in complex transportation conditions," *Journal of Low Frequency Noise Vibration and Active Control*, vol. 42, no. 2, pp. 509–524, 2023, doi: 10.1177/14613484221130197.
- [53] L. H. Zhao, H. C. Cai, T. Wang, and S. L. Zheng, "Durability assessment of automotive structures under random variable amplitude loading," *Advances in Mechanical Engineering*, vol. 10, no. 4, pp. 1–8, 2018, doi: 10.1177/1687814018771766.
- [54] W. S. Jie and S. A. Abu Bakar, "Dynamic Loading Effects on Car Suspension Components During Road Driving," *Journal of Transport System Engineering*, vol. 2, pp. 27–36, 2023, doi: 10.11113/jtse.v10.210.
- [55] T. C. Chan, A. Ullah, B. Roy, and S. L. Chang,

- "Finite element analysis and structure optimization of a gantry-type high-precision machine tool," *Scientific Reports*, vol. 13, no. 1, 2023. doi: 10.1038/s41598-023-40214-5.
- [56] X. Chen, Y. Liu, Q. Ma, P. Zhou, X. Liu, and J. Lin, "Finite element analysis of flexural performance of reinforced truss hollow composite concrete slabs," *Scientific Reports*, vol. 15, no. 1, pp. 1–19, 2025, doi: 10.1038/s41598-025-91209-3.
- [57] O. A. Adeyefa and O. O. Oluwole, "Finite Element Analysis of Von-Mises Stress Distribution in a Spherical Shell of Liquified Natural Gas (Lng) Pressure Vessels," *Engineering*, vol. 03, no. 10, pp. 1012–1017, 2011, doi: 10.4236/eng.2011.310125.
- [58] S. H. Park, A. B. Kareem, W. J. Joo, and J. W. Hur, "FEA Assessment of Contact Pressure and Von Mises Stress in Gasket Material Suitability for PEMFCs in Electric Vehicles," *Inventions*, vol. 8, no. 5, pp. 1–29, 2023, doi: 10.3390/inventions8050116.
- [59] K. Wang *et al.*, "Microstructural Evolution and Mechanical Properties of 7075 Aluminium Alloy during Semi-Solid Compression Deformation," *Crystals*, vol. 12, no. 8, 2022, doi: 10.3390/cryst12081119.
- [60] A. M. Khan, M. S. Khalil, and M. M. Azad, "Estimation of Vibration-Induced Fatigue Damage in a Tracked Vehicle Suspension Arm at Critical Locations Under Real-Time Random Excitations," *Machines*, vol. 13, no. 4, p. 257, Mar. 2025, doi: 10.3390/machines13040257.